Rotor Dynamics Test for Palmtop Gas Turbine Generator

Shuji Tanaka[1*], Kousuke Hikichi[2], Hiroshi Watanabe[2], Shinichi Togo[2], Masayoshi Esashi[1]
[1]Tohoku University, Department of Nanomechanics
6-6-01 Aza Aoba, Aramaki, Aoba-ku, Sendai 980-8579 Japan
[2]Tohoku-Gakuin University, Department of Mechanical Engineering
1-13-1 Chuo, Tagajo 985-8537, Japan

*Contact author: Tel: +81-22-795-6937, Fax: +81-22-795-6935, E-mail: shuji@cc.mech.tohoku.ac.jp

This paper reports rotor dynamics tests for a palmtop gas turbine generator, which generates several hundreds W for mobile robots. The designed rotor has the first bending resonant speed of 656000 rpm, which is higher than the rated rotation speed of 600000 rpm. However, the achieved rotation speed is only 480000 rpm, which is limited by the rotation-synchronous vibration of the rotor. We explained the reason that the actual resonant speed became approximately 20 % lower than the rated rotation speed using a nonlinear spring-mass model. The first resonant speed of the rotor must be higher than 120 % of the rated rotation speed, as recommended empirically.

Keywords: Gas turbine generator, Rotor dynamics, Nonlinear spring, Critical speed, Bearing

1 INTRODUCTION

A miniaturized gas turbine generator is one of major topics in the field of Power MEMS. There are two typical approaches: one is MEMS-based engine, which was first proposed by Epstein *et al.* [1], and the other is based on conventional mechanical machining technology. Our group have selected the latter approach to develop a palmtop gas turbine generator, which generates one to several hundreds W for mobile robots. Using 3-dimensional impellers with 10 mm diameter, we achieved the maximum rotation speed of 890000 rpm, which corresponds to a tip speed of 470 m/s [2], and then measured the compressor performance up to 720000 rpm [3], showing that such a small gas turbine is feasible from the view point of fluid dynamics.

The rotor used in the previous studies is made of titanium alloy, and does not include a generator magnet, because a lighter and shorter rotor is easier to rotate. For a practical palmtop gas turbine generator, however, the turbine impeller is made of nickel supper alloy, which is approximately twice as heavy as titanium alloy, and the rotor is equipped with a generator magnet. As a result, the rotor becomes heavy and long, and the rotor dynamics is one of the most critical issues. In this study, we designed a rotor for several hundreds W class gas turbine generator, and investigated the rotor dynamics by experiments and theoretical calculation.

2 DESIGN OF ROTOR

When the output of gas turbine generator is assumed, the size of impellers and a generator magnet can be determined. In this study, the diameter of the compressor and turbine impeller is 16 mm and 17 mm, respectively. The generator magnet is 14 mm in diameter and 20 mm in length including the containment ring. The purpose of this study is to find the rotor configuration which allows these three components to rotate at the rated rotation speed of 600000 rpm.

There are two typical layouts of the rotor as shown in Fig. 1. The first option is that the generator magnet is set between the turbine and compressor impeller. This layout is advantageous in rotor dynamics, because the overhangs from the bearings can be made short. In addition, the compressor can be maintained at low temperature, which is important to achieve high efficiency. Contrarily, the input of heat to the generator magnet from the turbine becomes large. A sophisticated cooling system is needed to keep the generator magnet blow 200 °C for samarium-cobalt magnet. The second option is that both turbine and compressor impeller overhang from one of the journal bearings. This layout is advantageous in cooling the generator, but has difficulty in the rotor dynamics and compressor efficiency. We have selected the first layout after experimental and theoretical investigations including the test of the cooling system.

From the dynamics of mechanical systems, the first bending resonant speed, N_{c1} must be larger than the rated rotation speed, N_r, ($N_r < N_{c1}$). Practically, it is empirically

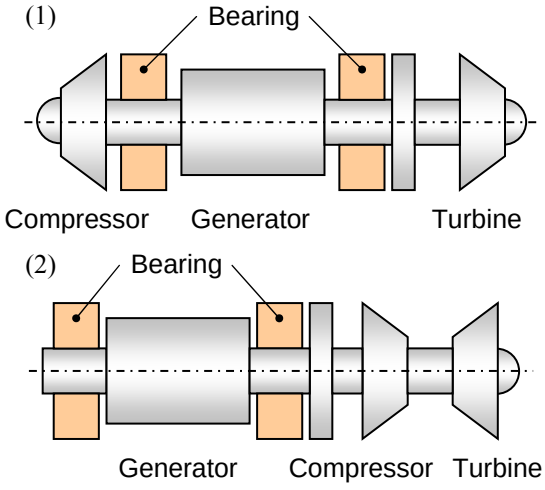

Figure 1 Typical layout of rotors.

recommended that the rated rotation speed leaves more than 20 % margin from the first bending resonant speed ($N_r \times 1.2 < N_{c1}$). This is referred as "120 % rule" in this paper.

We changed the dimensions of the rotor to find the solution which satisfies $N_r < N_{c1}$, preferably $N_r \times 1.2 < N_{c1}$. The resonant speeds were calculated by transfer matrix method. Figure 2 shows the structure of the rotor which we finally designed. Inconel 718 is selected as a material of the rotor for the first prototype engine. The calculated first bending resonant speed is shown in Fig. 3. It is approximately 656000 rpm, which is higher than the rated rotation speed of 600000 rpm, but leaves only 9 % margin.

If the diameter of the shaft is made larger, the first bending resonant speed decreases. However, the *DN* number (diameter in mm × rotation speed in rpm) and load of the journal bearing also increase. This makes the development of the bearings more difficult. In the present design shown in Fig. 2, the *DN* number reaches 4800000, and the weight of the rotor is 49 g. From the empirical trend between the maximum achievable rotation speed and the rotor weight per a single journal bearing shown in Fig. 4 [4], the weight of the rotor should be lower than 28 g (14 g × 2) to achieve 600000 rpm. This means that the designed rotor is already 75 % heavier than the empirical limitation. Therefore, we need to experimentally verify the maximum achievable rotation speed.

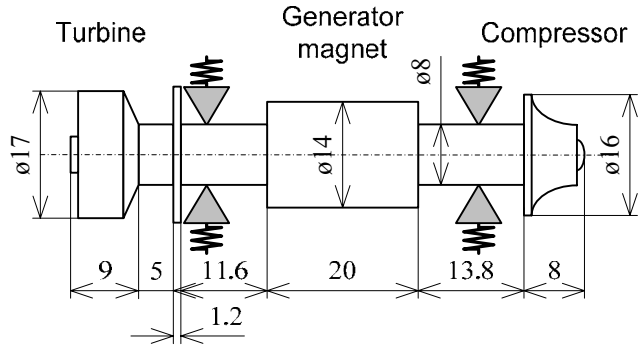

Figure 2 Structure of the designed rotor.

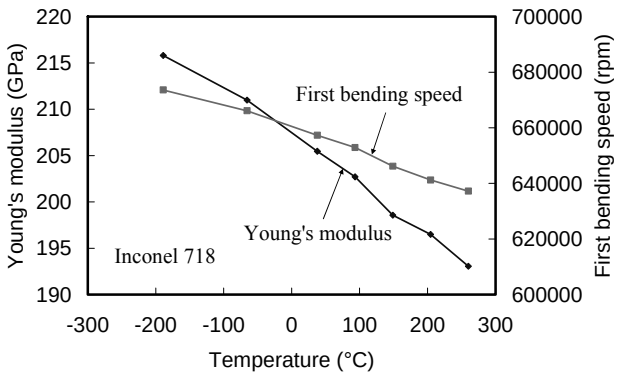

Figure3 Calculated first bending resonant speed vs. temperature.

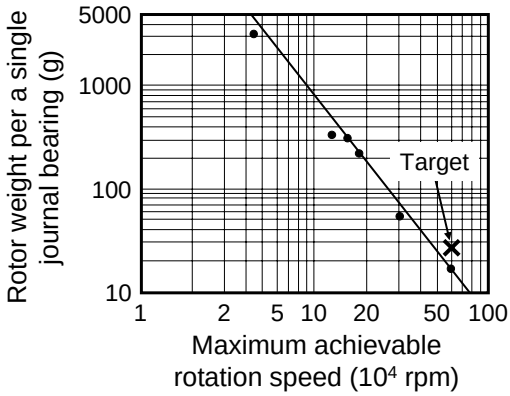

Figure 4 Empirical trend between the maximum achievable rotation speed and the rotor weight per a single journal bearing (reproduced from [4]).

3 ROTOR DYNAMICS TEST

3.1 Experimental Setup

The purpose of this experiment is to confirm the maximum achievable rotation speed of the rotor show in Fig. 2. For this purpose, the compressor impeller is not necessary, and thus exchanged to a dummy, which has the same weight and inertia. The generator magnet is also a dummy. Figure 5 shows the rotor, which is a single piece and made of Inconel 718.

As a journal and thrust bearing, hydroinertia air bearings, which we developed for the 10 mm diameter impellers [2, 5], are used. The journal bearing is a half-splitting type with a bearing gap of 30 μm, and made of zirconia ceramics. The estimated rigidity is 0.3 N/μm. The thrust bearing has a diameter of 18 mm, and is also made of zirconica ceramics. The estimated load capacity is 30 N, when the bearing gap reduces to 10 μm from an initial value of 30 μm.

Figure 6 shows the layout of the rotor and bearings. The motion of the rotor is measured in the radial direction at the center of the dummy magnet and in the axial direction at the end of the turbine impeller using Eddy current sensors. During the test, the rotor vibration is always monitored, and the test is stopped when the amplitude reaches a certain value to avoid the crash of the rotor to the bearings. The turbine is driven by compressed air at room temperature.

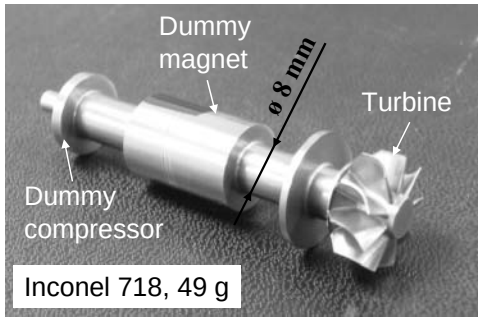

Figure 5 Rotor.

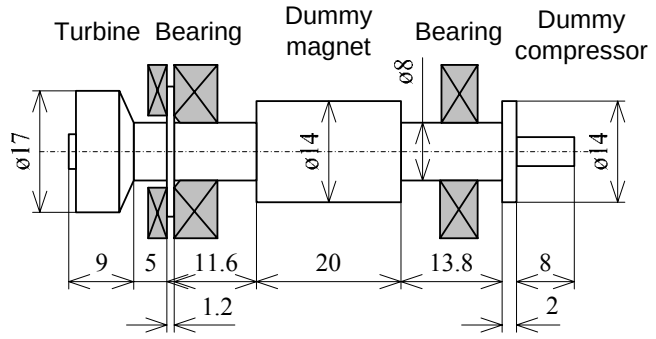

Figure 6 Layout of the rotor and bearings.

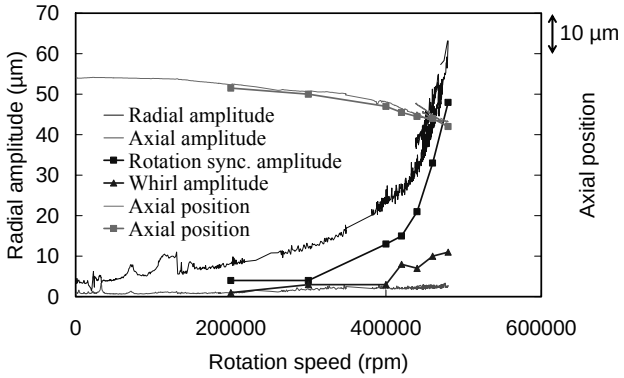

Figure 7 Radial amplitude and axial position of the rotor.

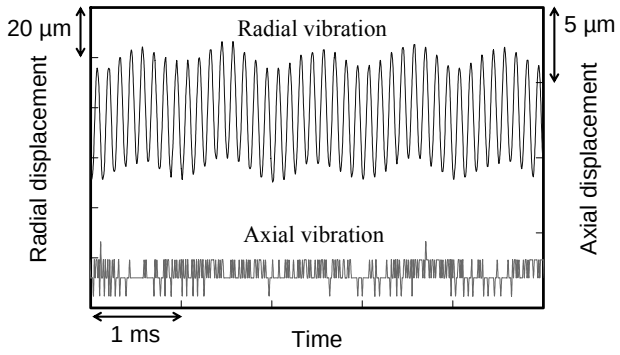

Figure 8 Waveform of the rotor vibration at 480000 rpm.

3.2 Experimental Result

We performed two times of test, before each of which the rotor was balanced to better than 0.5 g·μm. Figure 7 shows the radial amplitude and axial position of the rotor measured in the first test. The radial amplitude was as low as several microns until the rotation speed reached 300000 rpm, but it rapidly increased above 400000 rpm. When the radial amplitude reached 60 μm, and the test was stopped for safety. The achieved rotation speed is 480000 rpm and 460000 rpm for the first and second test, respectively.

Figure 8 shows the waveform of the rotor vibration at 480000 rpm for the first test. The waveform consists of two different frequencies: the higher one corresponds to rotation-synchronous vibration, and the lower one corresponds to whirl. We separated the radial amplitude shown in Fig. 7 into that of the rotation-synchronous vibration and whirl at seven representative rotation speeds. The results are plotted in Fig. 7. It is found that the amplitude of the rotation-synchronous vibration increased more rapidly than the whirl, limiting the maximum achievable rotation speed.

4 DISCUSSION

The rotation-synchronous vibration is excited by centrifugal force due to the unbalance of the rotor. The displacement of the rotation-synchronous vibration, x, at angular frequency ω follows the equation of motion:

$$m\ddot{x} + kx = me\omega^2 \sin \omega t \,, \tag{1}$$

where m, k and e is an equivalent mass, spring constant and unbalance, respectively. The particular solution of Eq. (1) is

$$x = e\frac{(\omega / p)^2}{1-(\omega / p)^2}\sin \omega t \,, \tag{2}$$

where $p = \sqrt{k/m}$. The first bending resonant frequency was predicted to be 656500 rpm at room temperature by the transfer matrix method, and thus $p = 2\pi \cdot 656500/60$. However, Eq. (2) is never fitted with the amplitudes of the rotation-synchronous vibration shown in Fig. 7, if $p = 2\pi \cdot 656500/60$. The best fitting was obtained when $p = 2\pi \cdot 540000/60$ (N_{c1} = 540000 rpm), as shown in Fig. 9. This means that the actual first bending resonant speed is approximately 20 % smaller than the predicted value. This result matches "120 % rule", but cannot be explained theoretically, because the error of the transfer matrix method is a several % at the maximum.

The change of the resonant frequency occurs, if a spring has nonlinearity. This effect is knows as "soft or hard spring effect". Now, we assume $k = \kappa + \beta x^2$, where κ is a constant and β represents nonlinearity. By substituting $k = \kappa + \beta x^2$ for Eq. (1), we obtain

$$\ddot{x} + p^2 x + \mu x^3 = e\omega^2 \sin \omega t \,, \tag{3}$$

where $\mu = \beta/m$. This is a nonlinear equation, and an approximate solution is found by the perturbation method. Now, we represent x by a power series of μ as

$$x = x_0 + \mu x_1 + \mu^2 x_2 + \ldots . \tag{4}$$

Also, p^2 is represented by a power series of μ as

$$p^2 = p_0^2 + \mu\alpha_1 + \mu^2\alpha_2 + \ldots . \tag{5}$$

By substituting Eq. (4) and (5) for Eq. (3),

$$\begin{aligned}&(\ddot{x}_0 + p_0^2 x) + \mu(\ddot{x}_1 + \alpha_1 x_0 + p_0^2 x_1 + x_0^3) \\ &+ \mu^2(\ddot{x}_2 + \alpha_2 x_0 + \alpha_1 x_1 + p_0^2 x_2 + 3x_0^2 x_1) + \ldots \\ &= e\omega^2 \sin \omega t\end{aligned} \tag{6}$$

is obtained.

Equation (6) is valid for any μ, and thus

$$\ddot{x}_0 + p_0^2 x_0 = e\omega^2 \sin \omega t \,, \tag{7}$$

$$\ddot{x}_1 + p_0^2 x_1 = -\alpha_1 x_0 - x_0^3 \quad \text{and} \tag{8}$$

$$\ddot{x}_2 + p_0^2 x_2 = -\alpha_2 x_0 - \alpha_1 x_1 - 3x_0^2 x_1 \quad (9)$$

The particular solution of Eq. (7) is

$$x_0 = e\frac{(\omega/p_0)^2}{1-(\omega/p_0)^2}\sin\omega t = A(\omega)\sin\omega t \cdot \quad (10)$$

By substituting Eq. (10) for Eq. (8),

$$\ddot{x}_1 + p_0^2 x_1 = -(\alpha_1 A(\omega) + \frac{3}{4}A^3(\omega))\sin\omega t + \frac{1}{4}A^3(\omega)\sin 3\omega t \quad (11)$$

is obtained. If $\omega \sim p_0$, the approximate general solution of Eq. (11) is given by

$$x_1 = C_1 \sin p_0 t + C_2 \cos p_0 t + (\alpha_1 A(\omega) + \frac{3}{4}A^3(\omega))\frac{t}{2\omega}\cos\omega t - \frac{A^3(\omega)}{32\omega^2}\sin 3\omega t \cdot \quad (12)$$

The third term monotonously increase with increase in t, but this does not occur actually. Therefore, the third term must be removed, and we obtain

$$\alpha_1 = -\frac{3}{4}A^2(\omega) \cdot \quad (13)$$

Under the boundary condition that $x_1(0) = 0$ and $\dot{x}_1(0) = 0$, Eq. (12) is solved as

$$x_1 = \frac{A^3(\omega)}{32\omega^2}(3\sin p_0 t - \sin 3\omega t) \cdot \quad (14)$$

Finally, the first approximation of the solution of Eq. (3) is obtained as

$$x = x_0 + \mu x_1 = A(\omega)\sin\omega t + \frac{\mu A^3(\omega)}{32\omega^2}(3\sin p_0 t - \sin 3\omega t) \cdot \quad (15)$$

Also, the substitution of Eq. (13) for Eq. (5) gives

$$p_0^2 = p^2 + \frac{3}{4}\mu A^2(\omega) = p^2 + \frac{3}{4}\mu\left(e\frac{(\omega/p_0)^2}{1-(\omega/p_0)^2}\right)^2 \cdot \quad (16)$$

Equation (16) show the dependency of the first resonant angular frequency, p_0, on ω. If $\mu < 0$, p_0 approaches ω with increase in ω, that is, the soft spring effect appears, because the amplitude of x increases according to Eq. (2). Equation (16) is numerically solved assuming $p_0 = \omega + 2\pi\cdot 10000/60$ (satisfying $\omega \sim p_0$), and Eq. (15) is fitted with the experimental result shown in Fig. 7. The best fitting is obtained, when $\mu = -0.5$ %/(10 μm)^2 and $p_0 = 2\pi\cdot 517400/60$ (N_0 = 517400 rpm), as shown in Fig. 10. From this discussion, we can conclude that the bending resonant speed can considerably decrease due to the nonlinearity of the equivalent rigidity of the rotor. However, the source of the nonlinearity is not clear.

5 CONCLUSION

We designed a rotor with a turbine impeller, compressor impeller and generator magnet for several hundreds W class gas turbine generator. The first bending resonant speed must be higher than the rated rotation speed theoretically, and empirically needs more than 20 % margin (120 % rule). The predicted first bending resonant speed is 656000 rpm, which is higher than the rated rotation speed of 600000 rpm, but leaves only 9 % margin.

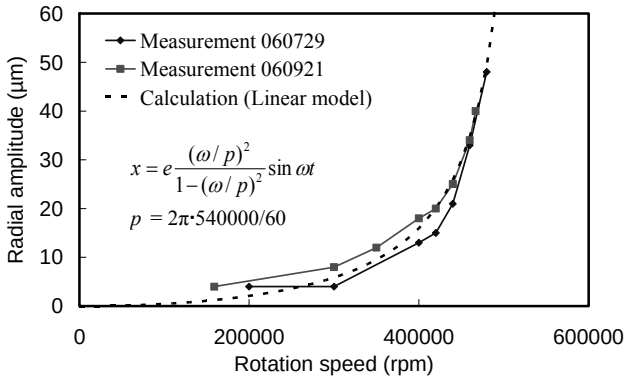

Figure 9 Amplitude of the rotation-synchronous vibration and fitting by a linear spring-mass model.

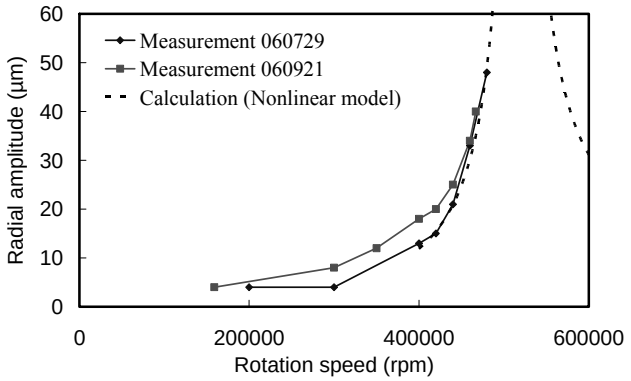

Figure 10 Amplitude of the rotation-synchronous vibration and fitting by a nonlinear spring-mass model.

The designed rotor is rotated using hydroinertia air bearings. The achieved rotation speed is 480000 rpm, which was limited by the rotation-synchronous vibration of the rotor. This result matches "120 % rule", but cannot be explained by a simple spring-mass model. In this study, we first gave a clear explanation to "120 % rule" by applying a nonlinear spring-mass model to the experimental result.

REFERENCES

[1] A. H. Epstein *et al.*, "Micro-Heat Engines, Gas Turbines, Rocket Engines – The MIT Microengine Project –", 28th AIAA Fluid Dynamics Conference, Snowmass Village, USA, June 29 – July 2, 1997, AIAA 97-1773.

[2] Shuji Tanaka *et al.*, "Hydroinertia Gas Bearing System to Achieve 470 m/s Tip Speed of 10 mm Diameter Impellers", *J. Tribology*, in press.

[3] Kousuke Isomura *et al.*, "Experimental verification of the feasibility of a 100W class micro-scale gas turbine at an impeller diameter of 10 mm", *J. Micromech. Microeng.*, 16 (2006) S254–S261.

[4] Shinichi Togo, "Air Bearing Design Handbook", Kyoritsu Shuppan (2002) 36, in Japanese.

[5] Kousuke Hikichi *et al.*, "Hydroinertia gas bearings for micro spinners", *J. Micromech. Microeng.*, 15 (2005) S171–S178.